Renewable Energy 151 (2020) 956–965

Contents lists available at ScienceDirect

Renewable Energy

journal homepage: www.elsevier.com/locate/renene

Three-dimensional modelling of suspended sediment transport in the far wake of tidal stream turbines

Xiaorong Li [a, b, *], Ming Li [b], Laurent O. Amoudry [c], Rafael Ramirez-Mendoza [c, d], Peter D. Thorne [c], Qingyang Song [e], Peng Zheng [b], Stephen M. Simmons [f], Laura-Beth Jordan [g, h], Stuart J. McLelland [h]

[a] School of Environmental Sciences, University of Liverpool, Liverpool, L69 7ZT, UK
[b] School of Engineering, University of Liverpool, Liverpool, L69 3GQ, UK
[c] National Oceanography Centre, Joseph Proudman Building, 6 Brownlow Street, Liverpool, L3 5DA, UK
[d] CICESE, Carretera Ensenada-Tijuana, No. 3918, Zona Playitas, Ensenada, BC, 22860, Mexico
[e] Institute for Space-Earth Environmental Research, Nagoya University, Nagoya, Aichi, 464-8601, Japan
[f] Energy and Environment Institute, University of Hull, Cottingham Road, Hull, HU6 7RX, UK
[g] School of Engineering, Institute for Energy Systems, The University of Edinburgh, Edinburgh, EH9 3DW, UK
[h] Department of Geography, Geology and Environment, University of Hull, Cottingham Road, Hull, HU6 7RX, UK

ARTICLE INFO

Article history:
Received 15 July 2017
Received in revised form
9 September 2019
Accepted 17 November 2019
Available online 25 November 2019

Keywords:
Tidal stream energy
Three-dimensional modelling
Suspended sediment transport
Mixing enhancement
Additional shear stress

ABSTRACT

A three-dimensional tidal turbine simulation based on an oceanographic numerical model has been tested for suspended sediment calculation, particularly in the wake of a standalone tidal turbine. The results suggest a need for further improvement of the model in order to obtain correct predictions of suspension strength of the wake and suspended sediment concentration under the influence of a turbine (compared to measured data). Due to the wide use of FVCOM in coastal applications where turbines are commonly installed, it proves necessary to address this issue. Two approaches with respect to modifying bed shear stress and turbulent mixing calculations in the presence of a turbine are proposed and tested in this research. Using data collected in the laboratory as reference, the turbulent mixing enhancement approach is shown to be effective. A series of tests are carried out to identify the impact of the turbine on suspended sediment transport in its vicinity. The results suggest that the impact is highly dependent upon the sediment grain size.

1. Introduction

As a potential resource of clean renewable energy, tidal stream energy has been gaining significant attention, particularly due to its predictability and widespread availability. However, the present understanding on impacts of such devices on the ocean environment is still in its infancy, with most of the understanding obtained through laboratory experiments and high resolution numerical simulations which restrict impact investigations to the near field. For example, porous discs [1–4] and scaled turbine prototypes [5,6] are used to study impacts of tidal turbines on the passing flow and turbulence. As a complementary tool to practical laboratory experiments, Computational Fluid Dynamics (CFD) modelling is also often used to investigate near field impacts of standalone turbines [7–10] and turbine arrays [11,12]. Despite the limitations of laboratory and CFD-based near field studies, they do provide properties of behaviours and impacts of single turbines which are critical inputs for large scale studies [13].

Flow dynamics in the near field can have a significant influence on local bed scour. In fact, the interaction between tidal stream energy devices and the local sediment environment has been identified as a key issue awaiting investigation [14,15]. Significant flow acceleration around the energy extraction site was observed in Ref. [7] which was believed to have increased bed scour [16]. Hence, three-dimensional simulations of a three-blade rotor operating at various depths (0.9D, 1.1D, 1.3D and 1.5D above the bed, where D is the diameter of the rotor) in a uniform flow was conducted by Ref. [16] using a CFD solver package OpenFOAM to reveal the impacts of a rotor on the three velocity components below the rotor

* Corresponding author. School of Environmental Sciences, University of Liverpool, Liverpool, L69 7ZT, UK.
E-mail address: lixr@liverpool.ac.uk (X. Li).

https://doi.org/10.1016/j.renene.2019.11.096

tip and the boundary layer in the near field. The results revealed that the maximum stream-wise velocity component below the rotor tip is around 1.07 times the velocity of the initial incoming flow and the flow rate within the boundary layer is also increased. While noting that the flow acceleration near the bed may result in an increased level of turbulence and larger bed shear stress which would cause transport of sediment, effects of the aforementioned changes on local bed scour are not quantified in Ref. [16].

Local scour associated with a fully operational turbine in terms of scour depth was quantified in Ref. [17]. Two experiments, clear water (bed shear stress below the critical value) and live-bed (local bed shear stress above the critical value), were carried out in a 15 m (L) and 0.9 m (W) tilting water flume. The diameter of the turbine was 0.15 m and the hub of the turbine was located 0.86D above the bed. It was reported that, after approximately 2.0–2.5 h of run time, the maximum scour depth of the clear water case was roughly 15 % of the rotor diameter and that of the live-bed case was 1.5 times deeper (roughly 24 % of the rotor diameter). Similar scour and sediment transport patterns were also observed in Refs. [6,18].

Two laboratory scale CFD cases were run in Ref. [19] to look at bed shear stress changes in the vicinity of two turbine rotors with different blockage ratios. In these two cases, the dimension of the flume was 3.7 m long, 4.2 m wide and 0.85 m deep. Diameter of the rotor was 0.5 m and it was placed at the mid-depth of the water. The two blockage ratios were 5.3% and 16%, respectively. The inlet flow speed was 0.9 m/s. It was found in this research that the bed shear stress of a large area in the vicinity of the rotor was affected. For the larger blockage case, along the centreline, the bed shear stress started to increase at −0.5D (0.5D upstream of the turbine) and the enhancement peaked at the turbine location (0D) due to flow diversion. A second peak of bed shear stress which was due to vortex generation was observed at 2.5D downstream of the turbine. The two peaks had roughly the same value and were about 9 times larger than the background bed shear stress (i.e. bed shear stress in the case without turbine). The investigation stopped at 6D downstream where the bed shear stress was still 6 times larger than the background value. The smaller blockage case demonstrated similar trend. But the overall stress was approximately 19% smaller than the larger blockage case.

On coastal scales, attention has also been given to the impacts of tidal turbines on sediment transport dynamics. A two-dimensional oceanographic model (depth-averaged) was applied to investigate the perturbation of turbine arrays on critical shear stress excess and flux difference between erosion and deposition in the Alderney Race [20]. Based on the results of a two-dimensional model with a resolution of 150 m in the vicinity of the turbines, it was concluded that the bed shear stress within the turbine farm was reduced by the presence of the devices. Two-dimensional oceanographic models with resolutions varying from 20 to 1000 m in the vicinity of turbine farms [21,22] were also built to explore impacts of turbine arrays on bed shear stress through case studies of sites with large tidal stream energy potential. Reduction of bed shear stress within the turbine array was also reported in these studies. This result, however, disagrees with the observations obtained through physical experiments and high resolution CFD simulations reviewed above. Also, based on a fine resolution (mesh size equals the diameter of the simulated turbine) three-dimensional oceanographic model, increased bed shear stress under the influence of a stand-alone turbine was reported in Ref. [23].

The above-mentioned disagreement is likely to be caused by using two-dimensional models in the regional scale studies [20–22]. The weakened bed shear stress reported in these studies was derived directly from depth-averaged water velocity which was reduced by the turbines. However, as observed in Ref. [16], velocity gradients within the boundary layer which largely control the bed shear stress could be increased due to the turbine in motion, despite the general reduction in depth-averaged velocity. Different scales used in the above-mentioned studies could also contribute to the disparity. Coastal-scale studies which used depth-averaged models and/or coarse mesh resolution (mesh size larger than the diameter of the simulated turbine, e.g Refs. [20–22]) investigated processes at array/regional scales, hence the array scale reductions in velocity were caused by 'global blockage' effects (i.e. regarding the turbine array as a whole). On the other hand, the laboratory/CFD studies and [23] focused on individual turbines and referred to their 'local blockage' effects.

Apart from velocity gradient in the bottom boundary layer and bed shear stress, turbulent mixing of the water is another important factor influencing sediment transport. Turbulent mixing was observed to be increased by a turbine in Ref. [5]. This could potentially enhance the suspension ability of the wake and hence the transport of suspended sediment. Again, complete turbulent mixing is unlikely to be captured in two-dimensional models [24,25]. It will also be missing in three-dimensional models if the turbulence closure is not modified [26].

As mentioned above, understanding impacts of tidal stream energy devices on regional scale is a critical aspect of the subject. To obtain such understanding, regional scale models are required because applications of models with smaller scales are often restricted to small spatial extents. However, fully resolving the turbine geometry in regional scale models is very unlikely and the effects of tidal turbines are often parameterised in such models (e.g. Refs. [23,27]). These parameterisations, however, focused on simulating impacts of tidal turbines on the flow and turbulent mixing, and their effectiveness on sediment transport have not been investigated. This work, therefore, aims to test the reliability of a newly developed three-dimensional regional model for tidal turbine simulation based on three-dimensional FVCOM [23] in simulating suspended sediment transport under the influence of tidal turbines. This is done by comparing results from numerical simulations with data collected from flume experiments [18]. The choice of the new model is based on the following considerations:

1. The numerical model of [23] is a regional scale model and, upon the completion of turbine parameterisation, it is suitable for applications that cover large geographical areas;
2. It includes three-dimensional representation of tidal turbine effects (see following section) which differs from previous studies and enables turbine effects on sediment suspension and transport to be simulated;
3. A new turbine-induced turbulence representation has been introduced in the new model [23] based on the existing 'MY-2.5' turbulent closure in FVCOM which is crucial for simulating the enhanced sediment mixing in the turbine wake.

Hence, further work on the model of [23] to incorporate impacts of turbines on sediment transport improves its capabilities in providing predictions of disturbances caused by tidal turbines on their surrounding environment.

2. Modelling system

2.1. 3D FVCOM

For the reason of simplicity, the basic theories and the parameterisation of turbines in the current and turbulent closure modules of FVCOM are not included here. For a thorough introduction, the readers may refer to Refs. [23,28]. The suspended sediment transport is calculated in FVCOM by integrating flow velocity and suspended sediment concentrations over the depth. The controlling

equation for the concentration-based suspended load calculation is as following:

$$\frac{\partial C_i}{\partial t}+\frac{\partial uC_i}{\partial x}+\frac{\partial vC_i}{\partial y}+\frac{\partial (w-w_i)C_i}{\partial z}=\frac{\partial}{\partial x}\left(A_H\frac{\partial C_i}{\partial x}\right)+\frac{\partial}{\partial y}\left(A_H\frac{\partial C_i}{\partial y}\right)+\frac{\partial}{\partial z}\left(K_h\frac{\partial C_i}{\partial z}\right) \quad (1)$$

where t is the time, x, y, and z are the east, north, and vertical axes in the Cartesian coordinate system; u, v, and w are the three velocity components in the x, y, and z directions respectively; C_i is the concentration of the *ith* sediment class; K_h the vertical eddy diffusivity; w_i the settling velocity of the *ith* sediment class and A_H the horizontal eddy viscosity given through the Smagorinsky eddy parameterisation.

$$A_H=\frac{0.5C_1\Omega^{\zeta}}{P_r}\sqrt{\left(\frac{\partial u}{\partial x}\right)^2+0.5\left(\frac{\partial v}{\partial x}+\frac{\partial u}{\partial y}\right)^2+\left(\frac{\partial v}{\partial y}\right)^2} \quad (2)$$

where C_1 is a constant parameter; Ω^{ζ} the area of the individual element and P_r the Prandtl number.

A sediment flux boundary condition is used at the bottom as:

$$K_h\frac{\partial C_i}{\partial z}=E_i-d_i \quad (3)$$

where E_i and d_i are the erosion and depositional rates respectively. The erosion rate E_i is calculated as following:

$$E_i=\triangle tQ_i(1-P_b)F_{bi}\left(\frac{\tau_b}{\tau_{ci}}-1\right) \quad (4)$$

where Q_i is the erosive flux; P_b the bed porosity; F_{bi} the fraction of the *ith* sediment class in the bottom; τ_b the bed shear stress and τ_{ci} the critical shear stress of the *ith* sediment class. The depositional rate d_i is calculated by solving the advection-diffusion equation.

2.2. Representation of turbines

Representation of turbines and their operation in the current and turbulence modules of FVCOM are reported in a previous paper by the authors in Ref. [23]. In particular, a layered change in the momentum extraction term across the turbine sweep area in the middle of the water column has been developed based on existing measurements and detailed CFD simulation results to represent the turbine-induced retarding effects. The three-dimensional flow field around the device and the adjacent wake region can therefore be simulated more realistically. The enhanced mixing effects are also included through added turbulence generation and dissipation terms with vertical variations as discussed in Ref. [23]. These new development forms the basis for the present study on sediment suspension behind the turbine in the far wake region.

Apart from impacts of turbines on current and turbulence discussed in Ref. [23], this study further hypothesizes that the rotation of a turbine affects the immediate sediment transport in two ways: (1) it increases the bed shear stress (τ_{bx} and τ_{by} in Section 2.1) and, consequently, the erosion of sediment and (2) it strengthens the suspension ability of the wake due to the enhanced vertical mixing (K_h in Equation (1) and K_m in the momentum equations − Equations (1)–(3) in Ref. [23]) caused by the rotating blades.

The additional bed shear stress (τ_r) caused by the rotation of the turbine is assumed to have a similar form as the equation to calculate bed shear stresses, i.e. $(\tau_{bx}, \tau_{by}) = C_d\sqrt{u^2+v^2}(u, v)$. Instead of flow velocity, it is based on the tip speed of the turbine in terms of m/s, U_r. It also takes the vertical location of the turbine into account and has the form as follows:

$$\tau_r=C_r{*}U_r^2{*}\frac{D}{h} \quad (5)$$

where h is the distance between the lower tip of the blade and the sea bed; C_r is a coefficient decided empirically through parameter studies, i.e. using trial and error to find C_r values that fit the predicted sediment concentration profiles to the observed ones. Multiple cases, utilising different numbers of τ_r are discussed in Section 3.3. As such, for the simplicity of the application, a simple linear combination of τ_b and τ_r is applied, leading to the total bed shear stress (τ_{bt}) as:

$$\tau_{bt}=\tau_b+\tau_r \quad (6)$$

The suspension ability of the water is reflected by K_h (see Equation (1)). The calculation of K_h is dependant on the turbulent closure which have been modified by Ref. [23] to account for the impacts of turbines on turbulence. Hence, the perturbation of turbines on the suspension ability of the wake have been taken into consideration in the predicted K_h indirectly. Whether or not this indirect modification is effective in terms of covering the impacts of tidal stream energy devices on the suspension ability of the wake is one of the focused problems discussed in this work.

3. Assessment of the three models

This section assesses the suspended sediment transport module of FVCOM under three scenarios:

1. With the turbine considered only in the current and turbulent closure modules of FVCOM according to Ref. [23] (Case 1 in Section 3.2. Detailed description of the cases mentioned in this section is also given in Table 1);
2. With its impacts on suspended sediment transport further reflected in bed shear stress according to Section 2.2 on top of scenario 1 (Cases 2 & 3 in Section 3.3);
3. With its impacts on suspended sediment transport further reflected in K_h calculations on top of scenario 1 (Case 4 in Section 3.4).

Note that the wave module is not activated in this research as the experimental data against which the model results are validated was collected under current-only conditions.

3.1. Model setup and calibration

To fulfil the above objective, an idealised model was built, recreating the experimental conditions of [18]. The computational domain is 11.0 m (length), 1.6 m (width) and 0.5 m (depth). The spatial resolution of the mesh is uniform throughout the domain with a mesh size of 0.2 m (i.e. one diameter of the turbine). Vertically, the water column is evenly divided into 50 sigma layers, and the turbine occupies a number of layers. Coefficients of turbine parameterisation in the current and turbulent closure modules can be found in Ref. [23]. The turbine hub is located 0.15 m above the bed and 4.0 m from the inlet of the flume to allow uniform flow to be fully developed. The time step of the model runs is 0.05 s and each model run has a spin up period of 10 min.

Model parameters associated with sediment transport are given in Table 2. Among the parameters, bottom roughness is estimated based on values reported in Ref. [18]. Settling velocity and critical stress are calculated based on the given D_{50} according to Van Rijn formulae [29]. The erosion flux (Q_i) is tuned according to the

Table 1
Detailed description of cases in Section 3.

Case No.	Modules modified to represent turbines		
	Current	Turbulence	Sediment transport
1	According to Ref. [23]	According to Ref. [23]	–
2	According to Ref. [23]	According to Ref. [23]	point source of τ_r
3	According to Ref. [23]	According to Ref. [23]	line source of τ_r
4	According to Ref. [23]	According to Ref. [23] + enhance K_h further	–

Table 2
Model parameters for suspended sediment calculation.

Model parameter	Value
Bottom roughness parameter (z_0)	0.0001 m
D_{50}	425 μm
Settling velocity	50.2 mm s^{-1}
Critical stress	0.2 N m^{-2}
Erosion flux (Q_i)	3×10^{-4} kg m^2 s^{-1}

measured suspended sediment concentration at the bottom at 15D downstream of the rotor (See Fig. 1 and its related discussion).

3.2. Assessment of the background model

A series of simulations are carried out to tune the erosion flux, Q_i, based on the settings given in Table 2. Comparison of suspended sediment concentration at 1 cm above the bed along the channel between the measured and calculated values when the erosion flux Q_i is set to 3×10^{-4} kg m^2 s^{-1} (Case 1) is presented in Fig. 1. Due to the lack of baseline measurements, sediment concentration in the bottom layer (the sigma layer closest to the bed in the model) at 15D downstream of the rotor measured in the laboratory is used as the reference to tune Q_i in the model (Fig. 2). It can be seen from Fig. 2 that the impact of the turbine on bed shear stress and, hence, sediment entrainment has dropped to a negligible level at 15D and beyond. Computed suspended concentration at 15D downstream of the rotor agrees very well with the measured value (Fig. 1), indicating a valid choice of Q_i. There is, however, obvious disagreement at the other locations. The calculated sediment concentration in the bottom layer is under-estimated in comparison with the laboratory measurements at the other 4 locations, potentially indicating an under-estimated bed shear stress in the wake of the turbine rotor.

Suspended sediment concentration profiles of Case 1 and the measured data at the 5 locations downstream of the rotor are drawn in Fig. 3. It is observed that even though the calculated concentration at the bottom layer of Case 1 is noticeably under-estimated at 5D downstream of the rotor, the concentration profile at 5D demonstrates a good agreement with the experimental data. However, sediment concentration in the water body drops rapidly and substantially under-estimated profiles are observed at the other 4 locations further downstream.

3.3. Assessment of additional bed shear stress

Hypothesising that the under-estimated suspended sediment profiles observed in Case 1 are caused by the under-predicted suspended sediment concentration at the bottom, two bed shear stress compensating cases are run (Cases 2 and 3). In each case the model is re-calibrated to fit the suspended sediment concentration profiles by altering C_r. In Case 2, τ_r is activated only at the turbine location with $C_r = 0.5$. In Case 3, τ_r is activated from -1D (1D upstream of the turbine location) to 12D in 14 linearly spaced increments, here C_r are 0.035, 0.0325, 0.03, 0.0275, 0.025, 0.0225, 0.02, 0.015, 0.01, 0.0075, 0.005, 0.0035, 0.002 and 0.001, respectively. The consideration of a large interval of the line source in Case 3 is to reflect the high stress zone observed downstream of the turbine in Ref. [19].

It can be seen from Fig. 1 that although by giving τ_r a large value at the turbine location might have increased the bottom sediment concentration immediately downstream of the turbine significantly, limited change is observed in the sediment concentration in the bottom layer beyond 5D downstream of the turbine. Compared to the almost negligible influence on the bottom sediment concentration beyond 5D, the C_r scheme of Case 2, however, does demonstrate a significant impact on the concentration profiles (see

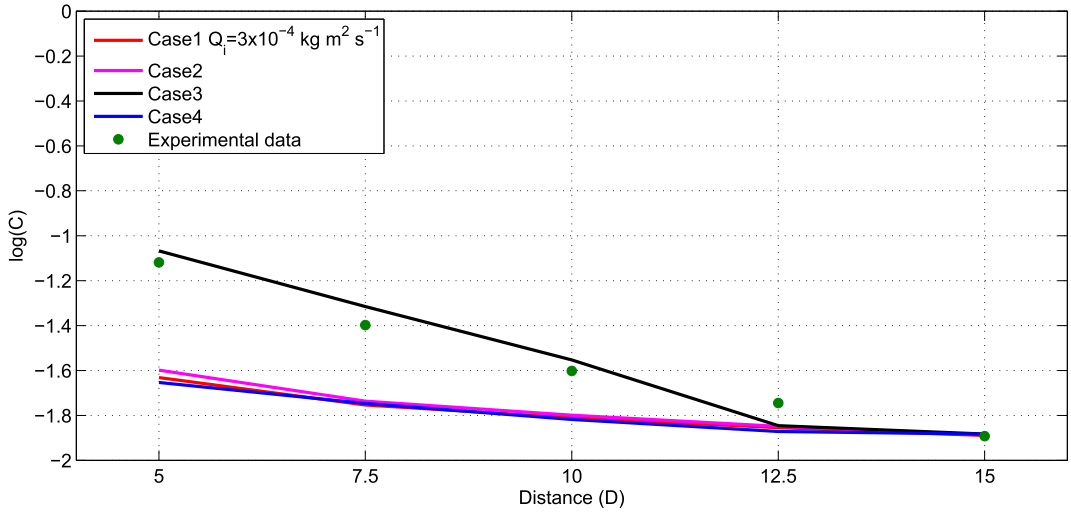

Fig. 1. Suspended sediment concentration at the bottom layer of cases 1–4.

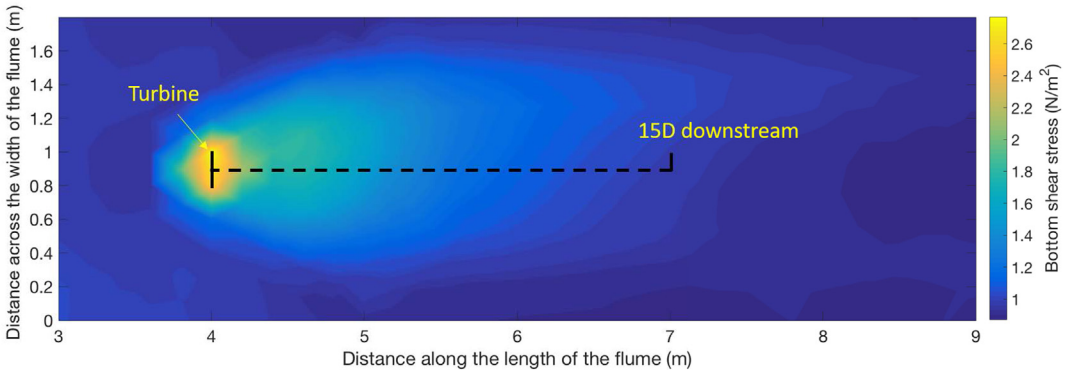

Fig. 2. Bed shear stress of Case 1.

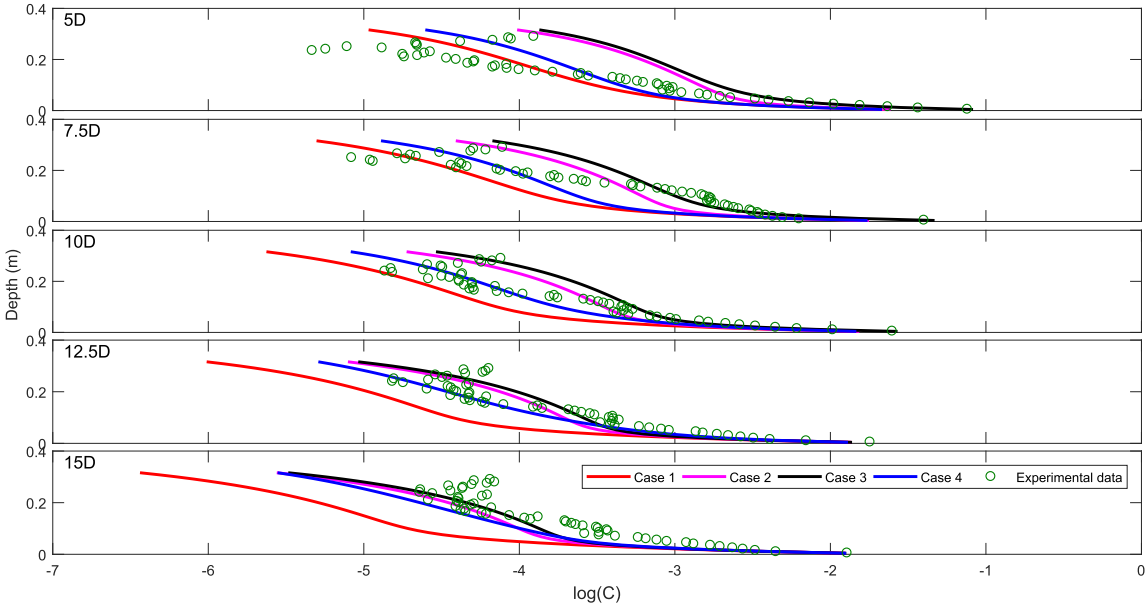

Fig. 3. Comparison of suspended sediment concentration profiles of cases 1–4.

Fig. 3). The profiles at 5D, 7.5D and 10D are greatly over-estimated. After a short period of satisfactory agreement at 12.5D, the profile at 15D starts to indicate a trend of under-estimation. This result suggests that the extra point source of sediment at the turbine location has largely enhanced the suspended sediment concentration in the water body close to the turbine. However, it should be noted that sediment concentration still drops rapidly with distance downstream.

Instead of a very strong point source, Case 3 represents a mild line source of extra bed shear stress and hence suspended sediment stretching from -1D to 12D. It can be seen from Fig. 1 that the calculated sediment concentration at the bottom layer of Case 3 agrees well with the measured result and is generally enhanced at the first 4 out of the 5 investigated locations compared to Case 1 and Case 2. Profile-wise, with a slightly over-estimated bottom sediment concentration at 5D, sediment profile at 5D is again over-estimated. Profiles at 7.5D and 10D are still over-estimated. Satisfactory agreement is obtained at 12.5D and 15D. However, again, rapid drop of sediment concentration in the water column is observed.

The fact that the sediment concentration profile at 5D downstream of the turbine produced by the background case (Case 1) is satisfactory and once there is extra bed shear stress source (i.e. additional τ_r) sediment concentration in the water body at 5D-10D is over-estimated suggests that the suspension ability of the water in the near wake of the turbine is at a correct to over-estimated level. However, the fast drop of sediment concentration beyond 5D observed in the above three cases strongly indicates an insufficient suspension strength in the far wake.

3.4. Assessment of enhanced K_h

This section details an exploratory test (Case 4) that aims to strengthen the suspension capability of the wake of the turbine by adjusting values of K_h in the far wake. In this case, K_h throughout the water column from 7D to 15D is enhanced by multiplying a linearly increasing coefficient from 1.55 to 1.7 which are obtained through parameter studies. The additional bed stress τ_r mentioned above is deactivated in this case to focus on the effects of enhanced suspension strength of the wake on sediment transport. Bottom sediment concentration and sediment profiles are again given respectively in Figs. 1 and 3. Without τ_r, sediment concentration at

the bottom is, as expected, under-estimated. The influence of enhancing K_h on bottom sediment concentration is negligible. However, it can be seen from Fig. 3 that by increasing K_h, sediment concentration in the far wake reduces at a lower rate and the concentration profiles are enhanced to a correct (compared to experimental data) level at all investigated locations. This method is therefore implemented in the large scale application below.

4. Application

A series of sediment tests are carried out in this section to reveal impacts of a single turbine on its surroundings based on a 15 m diameter turbine model. To represent flow conditions of a site with large tidal stream power potential — the Anglesey coast, North Wales, UK [30] — water depth for these cases was 45 m and the water velocity is 1.0 m/s. Spatially, the computational mesh has a uniform size of 15 m (i.e. one diameter of the turbine). Vertically, the water column is evenly divided into 50 sigma layers and, again, the turbine occupies a number of sigma layers. The turbine hub is located at the centre of water depth. The time step of the model runs is 1 s and each model run has a spin up period of 1 h. Four scenarios (descriptions are also given in Table 3) are considered: 1) undisturbed flow; 2) with turbine but without turbulent terms being activated (hereafter TbO); 3) with turbine and turbulent terms activated (hereafter TbM); and 4) with turbine and turbulent terms activated plus enhanced K_h (hereafter TbM + enhanced K_h). Note that for turbine representation in the current and turbulent closure modules, coefficients used in Ref. [23] are applied. Each scenario was run for a clear water case and a live-bed case. Parameters required for sediment calculations are listed in Table 4.

4.1. Bottom boundary layer

Fig. 4 compares water velocity, bed shear stress and suspended sediment concentration in the bottom boundary layer along the centreline of the test cases. It is observed from Fig. 4A that the presence of the turbine increases the water velocity in the bottom layer, regardless of the calculating scheme of turbulence. However, the increase is noticeably larger when the turbulent terms are activated (case TbM). Bed shear stress (Fig. 4B) which is largely dependant on water velocity in the bottom layer is also increased. The differences in bottom layer water velocity and bed shear stress caused by the turbulence calculating scheme starts to become negligible beyond 10D downstream of the turbine.

Suspended sediment concentration in the bottom layer demonstrates opposite responses to the inclusion of turbine and turbulent terms in the clear water (Fig. 4C) and live-bed (Fig. 4D) cases. It can be seen from Fig. 4C that in the clear water case, the bed shear stress under the undisturbed flow is below the critical stress, thus sediment concentration in the bottom layer is 0 $kg/\ m^3$. However, bed shear stress in case TbO is enhanced due to the inclusion of a turbine, and it is above the critical stress, entraining sediment particles into the water column. Sediment concentration in the bottom layer is even higher in case TbM, where the bed shear stress is further enhanced in comparison with case TbO.

Table 4
Model parameter meters for suspended sediment calculation.

Model parameter	live-bed	clear water
D_{50}	0.22 mm	4.00 mm
Settling velocity	21.0 mm s^{-1}	250.3 mm s^{-1}
Critical stress	0.154 N m^{-2}	2.400 N m^{-2}

It is, however, a very different scenario in the live-bed case (Fig. 4D). Suspended sediment concentration in the bottom layer is decreased in case TbM in the vicinity of the turbine. This result could be counter-intuitive, given an enhanced bed shear stress within the same area. However, apart from bed shear stress, turbulent mixing close to the device is also increased due to the inclusion of the turbine, especially in case TbM. The enhanced mixing is able to mix sediment concentration into a more uniform state close to the bed surface where the concentration is high. In this particular case, the enhanced bed shear stress and hence increased sediment supply from the bed is not enough to compensate for the amount of sediment being transported upwards out of the bottom layer due to the mixing process; suspended sediment concentration in the bottom layer is therefore decreased.

The distribution of suspended sediment concentration along the water channel in case TbO is not exactly the same. The sharp drop of suspended sediment concentration in the vicinity of the turbine seen in case TbM is not observed in case TbO. Instead, only a very slight decrease of suspended sediment concentration is observed at -1D. This is because, without the turbulence modification terms, the turbulent mixing level in case TbO in the vicinity of the turbine is much lower, and hence less sediment is being transported upwards out of the bottom layer. At 0D, sediment concentration in the bottom boundary layer has a very similar value to that in the undisturbed case. It then rises above the concentration of the undisturbed case beyond 1D downstream of the turbine. From 3D downstream of the turbine, suspended sediment concentration in all three cases demonstrates a similar behaviour as that observed in the clear water test: concentration is the highest in case TbM, its value in case TbO is in the middle and it is the lowest in the undisturbed case. This is because the turbulent mixing is gradually recovering to the undisturbed level in the wake. From 3D downstream of the turbine, the mixing level in both turbine present cases has dropped to an extent where the amount of sediment being transported upwards out of the bottom layer is smaller than that being picked up from the bed into the bottom layer through erosion. Under such circumstances, larger bed shear stress leads to stronger erosion and therefore higher suspended sediment concentration in the bottom layer.

The enhancement of K_h on the basis of case TbM results in reduced suspended sediment concentration in the bottom layer in both clear water and live-bed tests, for the same reason explained above. The impact of enhanced K_h on suspended sediment is small in the clear water test, due to the large settling velocity of the sediment applied in this test. On the other hand, the enhanced K_h

Table 3
Detailed description of scenarios in Section 4.

Scenarios	Modules modified to represent turbines	
	Current	Turbulence
Undisturbed flow	–	–
TbO	According to Ref. [23]	–
TbM	According to Ref. [23]	According to Ref. [23]
TbM + enhanced K_h	According to Ref. [23]	According to Ref. [23] + enhance K_h further

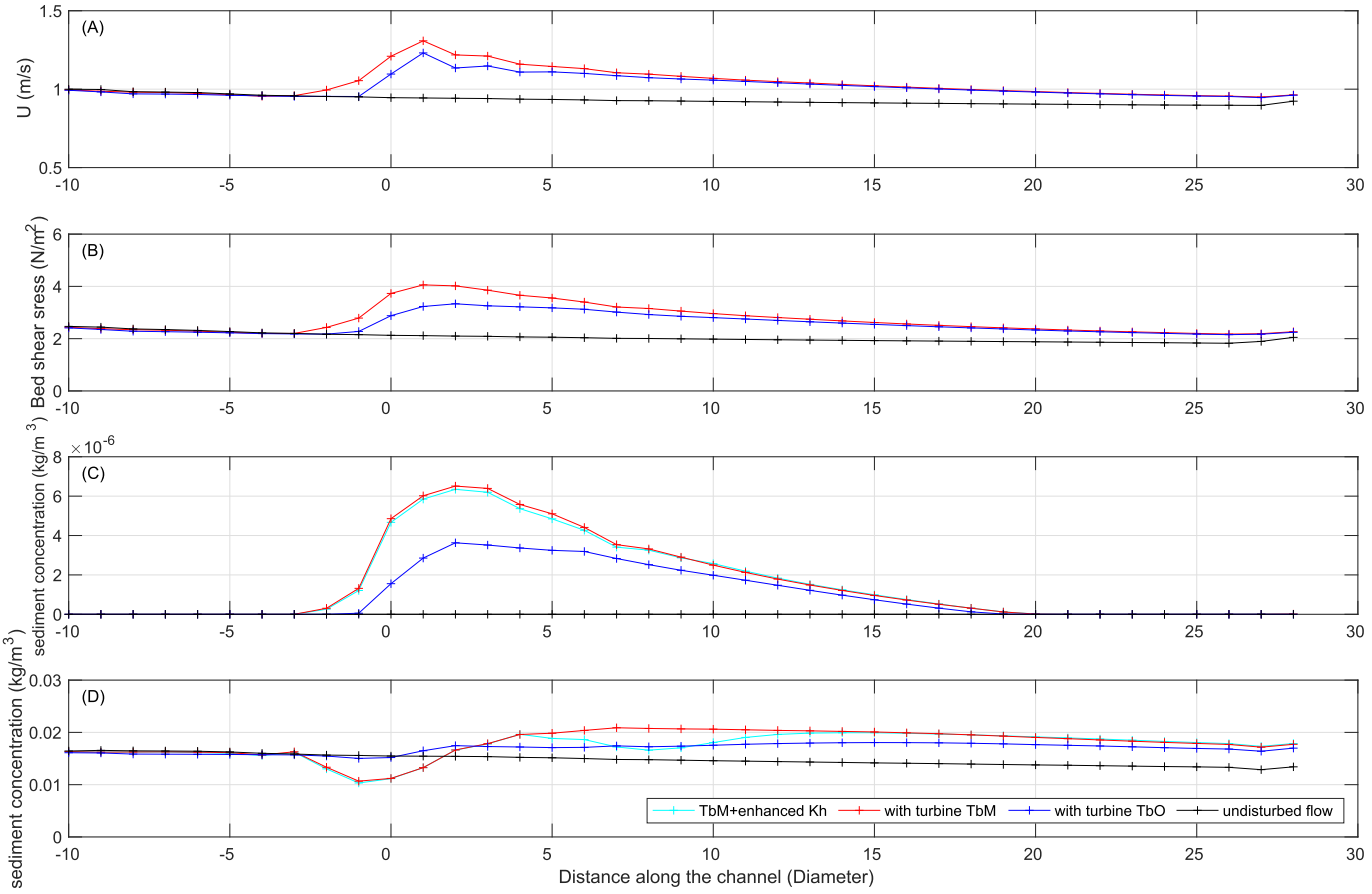

Fig. 4. (A) Water velocity in the bottom layer, (B) Bed shear stress, (C) Suspended sediment concentration in the bottom layer along the centreline of a clear water case and (D) Suspended sediment concentration in the bottom layer along the centreline of a live-bed case calculated under different scenarios: TbM + enhanced K_h — turbine + turbulent terms + enhanced Kh, TbM — turbine + turbulent terms, TbO — turbine and undisturbed flow.

has an obvious impact on suspended sediment concentration in the bottom layer in the live-bed test in which the settling velocity of the sediment particles is lower. Suspended sediment concentration in the bottom layer between 5D and 15D of the live-bed test is reduced compared to case TbM. The further increased mixing within this region, on top of the enhancement caused by the inclusion of a retarding force and activation of turbulent terms (see Ref. [23] for details), increases the amount of sediment being transported upwards out of the bottom layer and hence reduces the sediment concentration in the bottom layer at these locations.

4.2. Suspended sediment distribution across water depth

Fig. 5 demonstrates suspended sediment concentration throughout the water depth of the clear water test case calculated under the above-mentioned four scenarios: TbM + enhanced K_h, TbM, TbO and undisturbed water. Clearly, due to the size of the particles, vertical transport of sediment from the seabed upwards is very limited. Suspended sediment transport is restricted to the very bottom layers.

Suspended sediment concentration throughout the water depth of the live-bed test calculated under the four aforementioned scenarios is presented in Fig. 6. It is observed that sediment suspension is largely restricted to the lower body of the water in the undisturbed flow. Sediment concentration remains constant in this case. Changes in suspension are clearly seen in the other three cases where the turbine is present. Consistent with results discussed in Fig. 4, sediment concentration close to the bottom around the turbine is obviously reduced in cases TbM + enhanced K_h and TbM, while changes in concentration within the same region in case TbO is less apparent. Sediment concentration close to the bed further downstream is observed to be increased in all turbine present cases. The decrease in bottom layer sediment concentration at locations 5D-15D in Case TbM + enhanced K_h in comparison to Case TbM is also observed.

Apart from changes incurred to suspended sediment distribution close to the bed, sediment concentration at the upper part of the water column is also affected. It can be seen from Fig. 6 that the inclusion of the turbine clearly enhances the turbulence induced mixing and results in a higher sediment concentration in the upper part of the water column in all turbine present cases. Between Case TbM and Case TbO, the enhancement is more apparent in Case TbM where the turbulent terms are activated, resulting in a higher mixing level of the wake. Between Case TbM + enhanced K_h and Case TbM, suspended sediment concentration at the upper part of the water body is higher in Case TbM + enhanced K_h due to the adjustment of K_h.

5. Discussions

Using a newly developed three-dimensional regional model for tidal turbine simulation which includes turbines in the current and turbulent closure modules of three-dimensional FVCOM [23], this work aims to simulate sediment transport in the far wake of a standalone tidal turbine using a large scale three-dimensional model with fine mesh resolution. Through comparing model

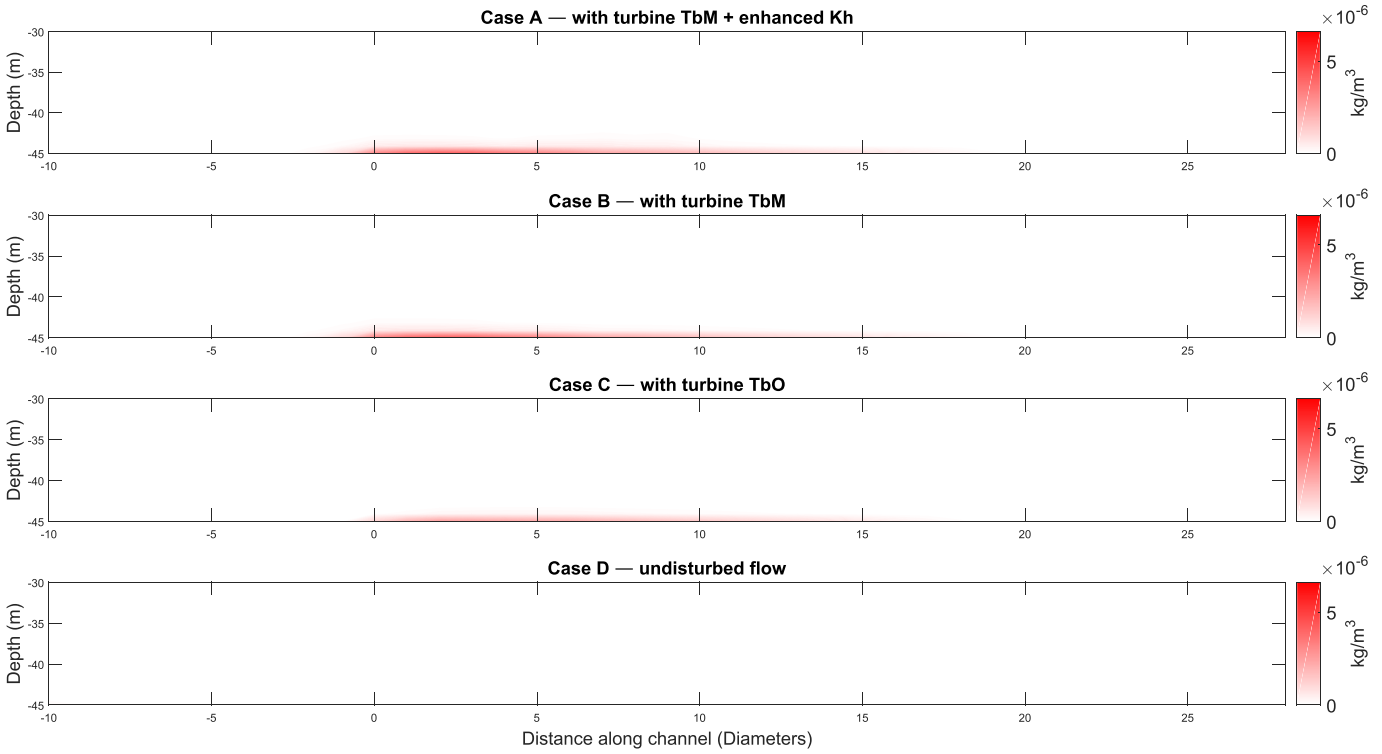

Fig. 5. Suspended sediment concentration contours of the clear water test: Case A — TbM + enhanced K_h, Case B — TbM, Case C – TbO and Case D — undisturbed flow.

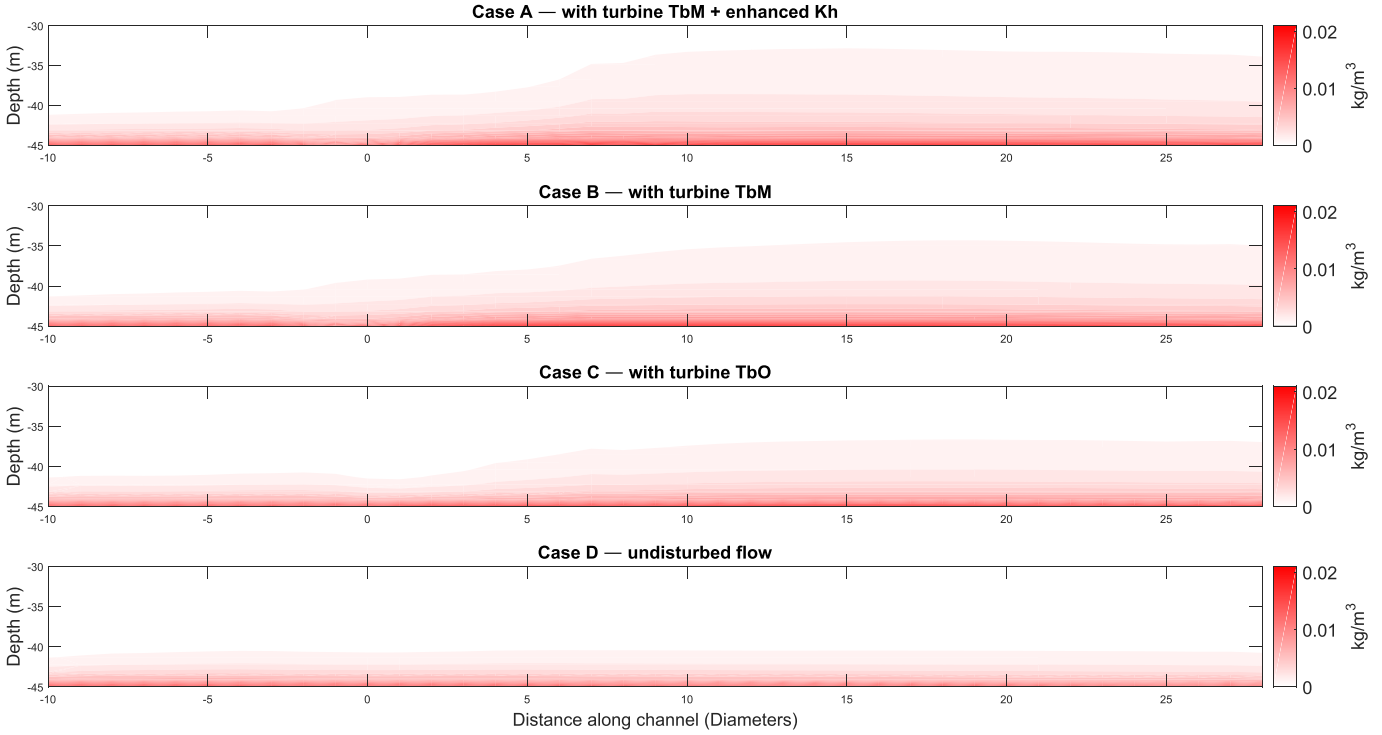

Fig. 6. Suspended sediment concentration contours of the live-bed test: Case A (TbM) —with turbine and with turbulent terms being activated, Case B (TbO) —with turbine but without turbulent terms being activated and Case C —undisturbed flow.

predictions to data collected in the laboratory (Fig. 3), results show that, without further modification made to the model, suspended sediment concentration in the far wake is under-estimated (e.g. by ∼ 54% at 10D and ∼ 65% at 15D downstream of the turbine). This is likely to be caused by insufficient suspension strength of the wake predicted by the model. Approaches for achieving correct level of predictions are proposed and tested. Test results suggest that further treatment to the vertical mixing (K_h) of the model can be an

effective solution. By enhancing K_h in the far wake, profiles of suspended sediment concentration agree well with the observed ones. Root mean square error percentages ($\%_{RMSE}$ as calculated in Ref. [23]) at 10D and 15D are 3.8 and 6.6, respectively.

There are two possible reasons for the requirement of further treatment to K_h in order to obtain a correct prediction of suspended sediment in the far wake of a tidal turbine. First, the turbulent closure ('MY-2.5') used in the vertical direction relates turbulence stresses to the mean flow and hence fails to capture the fluctuation of the turbulent flow. Interactions between turbulent flow and sediment particles [31], therefore, are not fully resolved. Second, the eddy viscosity theory is used to parameterize turbulence in a continuous fluid medium like water. However, sediment particles should be considered as discrete elements unless they are very fine (finer than cohesive mud which is unlikely at potential sites for introduction of tidal turbine farms). Therefore, K_h calculated by the turbulent closure could be unsuitable for describing diffusive behaviours of sediment particles, especially particles in strong swirling fluids. In a like manner, modification of K_h calculation has been suggested to obtain good predictions of suspended sediment concentrations above rippled beds (e.g. Ref. [32]).

Apart from the necessity of further mixing enhancement in the far wake of a turbine in the model for accurate prediction of sediment suspension of the wake, model application results based upon clear water and live-bed tests suggest the important role of sediment size in determining effects of tidal turbines. It is expected that under a given hydrodynamic conditions at a site, finer sediment behave differently from coarser sediment due to the competition between enhanced entrainment, enhanced mixing as well as settling in the water column as the present model results indicate. The resultant long term morphological changes in the far field therefore is often complex to analyse.

It should be noted that the parameterisation for impact of turbines on sediment transport described herein is based on previously validated parameterisation for turbines' impact on flow and turbulence (i.e. [23]), small errors in the previous parameterisation could be cascaded down to the work described herein. Also, the experimental data based on which the numerical cases are tested was collected after equilibrium was reached, during which a scour pit of 0.04 m occurred below the turbine [18]. This morphological change is not reflected in the model and could have contributed to the above-mentioned discrepancies between the model predictions and the experimental data. The discrepancies could also be attributed to the use of uniform particle size in the model, as in the experiment mixed sediment size was used (see Fig. 2 in Ref. [18]). Further, assessment of the model is based on the application of a regional scale model to a flume which may impose constrains on the fundamental assumptions of the numerical model. Comparison between results from coastal ocean models and data collected from large-scale flume experiments is, however, a commonly accepted approach to test the reliability of model results (e.g. Refs. [33,34]).

Aiming to provide a numerical tool that can be applied to real world scale array simulations, an oceanographic model (FVCOM) is used in this research. FVCOM uses a RANS-based turbulence model to simulate turbulent flows in the vertical direction, and a LES-based (Large Eddy Simulations) model on the horizontal directions. LES models filter turbulent processes smaller than the mesh size, hence generally horizontal mesh size needs to be finer than the scale of target process to allow a LES model to give sensible results. Due to the computational effort required by real world scale array simulations, horizontal mesh sizes of cases described in this research are limited to the size of the turbine. This is justifiable because the model is found to be insensitive to horizontal mixing through a sensitivity test (see Fig. 7). However, it should be noted that for a different modelling system that can have a finer presentation of the turbine (e.g. CFD models) or an oceanographic model that resolves turbine/arrays at a different mesh resolution, re-assessment on the requirement of the above-mentioned model improvements and re-calibration on the coefficients used may be needed. Necessities of coefficient re-calibration may also be incurred by changes of dimension and location of the turbine as they affect the wake structure (e.g. Refs. [3,6]).

Regarding the formulation of the additional retarding force used to simulate deceleration of the passing flow caused by energy extraction and blockage effect of tidal turbines [23], it was pointed out in Refs. [13,27] that the credibility of the additional retarding force term is under question in relation to the choice of velocity in the application (local vs. upstream velocities), particularly when the mesh size is the same scale as the turbine, which is the case in this research. To address this, a correction to regulate discrepancies caused by using local or upstream velocities was proposed in Ref. [13]. Note that as this correction is not applied in this research, the applicability of the related coefficient (C_{ext} in Ref. [23]) calibrated in one case may be restricted to the mesh size/turbine size ratio used.

Nevertheless, our numerical experiments demonstrate the necessity for modifications to a RANS-based turbulence model, 'MY-2.5', embedded in a large scale oceanography model in order to achieve accurate predictions of sediment suspension strength of

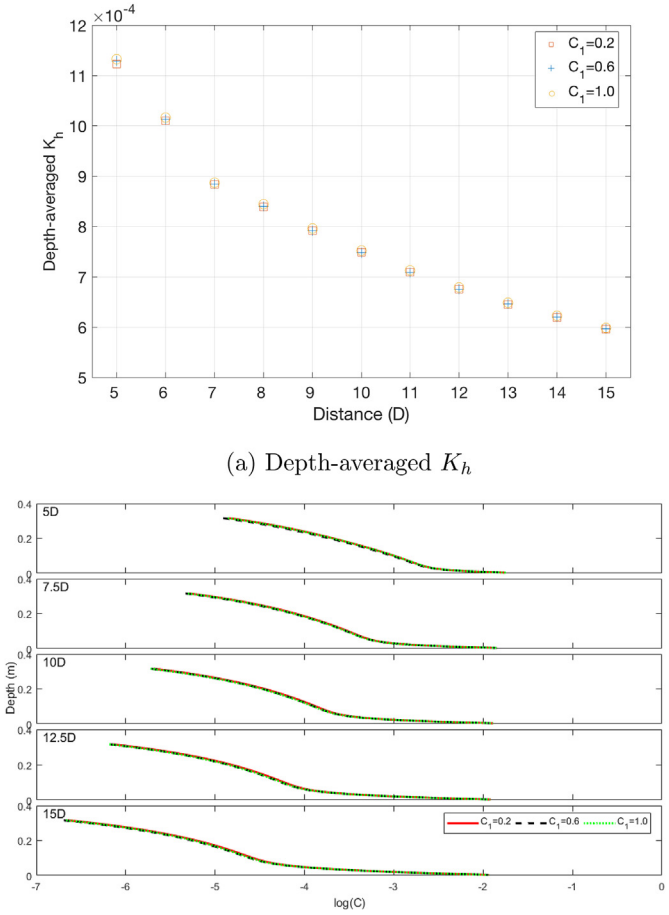

(a) Depth-averaged K_h

(b) Suspended sediment concentration

Fig. 7. Sensitivity test based on Case 2 described in Section 3.3. With C_1 in Equation (2) varying from 0.2 to 1.0, depth-averaged K_h changed ~ 1 %at 5D downstream of the turbine.

the wake and, hence, accurate predictions of sediment transport dynamics due to the influence of tidal turbines. Through these tests, we also found a competing mechanism between turbine-induced enhanced sediment entrainment and enhanced mixing which is particularly relevant to sediment in suspended transport.

6. Conclusions

Without any further modification, the inclusion of turbine rotor in the current and turbulence modules is able to produce an enhanced level of suspended sediment at 5D downstream of the turbine. However, suspended sediment concentration further downstream is significantly under-estimated. Under-prediction is also observed in sediment concentration at the bottom layer. Activating the additional bed shear stress term, especially as a line source, can lead to a good agreement in sediment concentration at the bottom. This, however, causes sediment concentration in the water body to be largely over-estimated at 5D, 7.5D and 10D downstream of the turbine. Also, sediment concentration in the water body drops very quickly beyond 5D, indicating an under-estimated suspension strength of the far wake. By solely enhancing K_h in the far wake, reasonable profiles are obtained, despite under-estimated sediment concentration at the bottom.

The influences of turbine operation on sediment suspension is not always the same. In the clear water condition, both the enhanced bed shear stress and turbulent mixing tend to increase the sediment suspension and hence lead to a rise in sediment concentration. On the contrary, in the live-bed condition, even though the increase in bed shear stress entrains more sediment from the bed surface into the water column, the enhanced vertical mixing demands a higher level of sediment supply from the bed. With the right gain size, starvation of sediment in suspension is seen under these two competing mechanisms, which leads to the reduction of concentration near the bottom. It is therefore noted that the sediment grain size attributes to the fundamental effects on the results.

Acknowledgement

The current study is supported by the Chinese Scholar Council and the University of Liverpool. The authors are grateful to Richard D. Cooke and Brendan Murphy for their help setting-up and running the experiments using the Total Environment Simulator at the University of Hull, results of which were used to validate this work. The authors would also like to acknowledge funding from the Engineering and Physical Sciences Research Council (EPSRC) to grant EP/J010359/1 (Interactions of flow, tidal stream turbines and local sediment bed under combined waves and tidal conditions), which is part of the Supergen consortium.

References

[1] A. Bahaj, L. Myers, M. Thomson, N. Jorge, Characterising the wake of horizontal axis marine current turbines, in: Proceedings of the 7th European Wave and Tidal Energy Conference, Port, Portugal, 2007.
[2] L. Myers, A. Bahaj, An experimental investigation simulating flow effects in first generation marine current energy converter arrays, Renew. Energy 37 (1) (2012) 28–36.
[3] L. Myers, A. Bahaj, Experimental analysis of the flow field around horizontal axis tidal turbines by use of scale mesh disk rotor simulators, Ocean. Eng. 37 (2) (2010) 218–227.
[4] F. Maganga, G. Germain, J. King, G. Pinon, E. Rivoalen, Experimental characterisation of flow effects on marine current turbine behaviour and on its wake properties, IET Renew. Power Gener. 4 (6) (2010) 498–509.
[5] S. Tedds, I. Owen, R. Poole, Near-wake characteristics of a model horizontal axis tidal stream turbine, Renew. Energy 63 (2014) 222–235.
[6] L.B. Jordan, S. Simmons, S. McLelland, B. Murphy, D. Parsons, L. Vybulkova, The impact of tidal stream turbines on 3D flow and bed shear stress measured with particle image velocimetry in a laboratory flume, in: Proceedings of the 11th European Wave and Tidal Energy Conference, Nantes, France, 2015, pp. 654–660.
[7] X. Sun, J. Chick, I. Bryden, Laboratory-scale simulation of energy extraction from tidal currents, Renew. Energy 33 (6) (2008) 1267–1274.
[8] M. Harrison, W. Batten, L. Myers, A. Bahaj, Comparison between CFD simulations and experiments for predicting the far wake of horizontal axis tidal turbines, IET Renew. Power Gener. 4 (6) (2010) 613–627.
[9] X. Bai, E. Avital, A. Munjiza, J. Williams, Numerical simulation of a marine current turbine in free surface flow, Renew. Energy 63 (2014) 715–723.
[10] A. Goude, O. Ågren, Simulations of a vertical axis turbine in a channel, Renew. Energy 63 (2014) 477–485.
[11] L. Bai, R.R. Spence, G. Dudziak, Investigation of the influence of array arrangement and spacing on tidal energy converter (TEC) performance using a 3-dimensional CFD model, in: Proceedings of the 8th European Wave and Tidal Energy Conference, Uppsala, Sweden, 2009, pp. 654–660.
[12] R. Malki, I. Masters, A.J. Williams, T.N. Croft, Planning tidal stream turbine array layouts using a coupled blade element momentum–computational fluid dynamics model, Renew. Energy 63 (2014) 46–54.
[13] S.C. Kramer, M.D. Piggott, A correction to the enhanced bottom drag parameterisation of tidal turbines, Renew. Energy 92 (2016) 385–396.
[14] G. Cada, J. Ahlgrimm, M. Bahleda, T. Bigford, S.D. Stavrakas, D. Hall, R. Moursund, M. Sale, Potential impacts of hydrokinetic and wave energy conversion technologies on aquatic environments, Fisheries 32 (4) (2007) 174–181.
[15] L. Chen, R. Hashim, F. Othman, S. Motamedi, Experimental study on scour profile of pile-supported horizontal axis tidal current turbine, Renew. Energy 114 (2017) 744–754.
[16] L. Chen, W.-H. Lam, Slipstream between marine current turbine and seabed, Energy 68 (2014) 801–810.
[17] C. Hill, M. Musa, L.P. Chamorro, C. Ellis, M. Guala, Local scour around a model hydrokinetic turbine in an erodible channel, J. Hydraul. Eng. 140 (8) (2014), 04014037.
[18] R. Ramírez-Mendoza, L. Amoudry, P. Thorne, R. Cooke, S. McLelland, L. Jordan, S. Simmons, D. Parsons, L. Murdoch, Laboratory study on the effects of hydro kinetic turbines on hydrodynamics and sediment dynamics, Renew. Energy 129 (2018) 271–284.
[19] S. Sufian, Ph.D. thesis, Numerical Modeling of Impacts from Horizontal axis Tidal Turbines, vol. 6, School of Engineering, University of Liverpool, 2016.
[20] J. Thiébot, P.B. du Bois, S. Guillou, Numerical modeling of the effect of tidal stream turbines on the hydrodynamics and the sediment transport–application to the Alderney Race (Raz Blanchard), France, Renew. Energy 75 (2015) 356–365.
[21] R. Martin-Short, J. Hill, S. Kramer, A. Avdis, P. Allison, M. Piggott, Tidal resource extraction in the Pentland Firth, UK: potential impacts on flow regime and sediment transport in the Inner Sound of Stroma, Renew. Energy 76 (2015) 596–607.
[22] D. Haverson, J. Bacon, H.C. Smith, V. Venugopal, Q. Xiao, Modelling the hydrodynamic and morphological impacts of a tidal stream development in ramsey sound, Renew. Energy 126 (2018) 876–887.
[23] X. Li, M. Li, S.J. McLelland, L.-B. Jordan, S.M. Simmons, L.O. Amoudry, R. Ramirez-Mendoza, P.D. Thorne, Modelling tidal stream turbines in a three-dimensional wave-current fully coupled oceanographic model, Renew. Energy 114 (2017) 297–307.
[24] I. Bryden, S. Couch, A. Owen, G. Melville, Tidal current resource assessment, Proc Inst Mech Eng A J Power Energy 221 (2) (2007) 125–135.
[25] S. Serhadlıoğlu, T.A. Adcock, G.T. Houlsby, S. Draper, A.G. Borthwick, Tidal stream energy resource assessment of the Anglesey Skerries, Int. J. Mar. Energy 3 (2013) e98–e111.
[26] M. De Dominicis, R.O. Murray, J. Wolf, Multi-scale ocean response to a large tidal stream turbine array, Renew. Energy 114 (2017) 1160–1179.
[27] T. Roc, D.C. Conley, D. Greaves, Methodology for tidal turbine representation in ocean circulation model, Renew. Energy 51 (2013) 448–464.
[28] C. Chen, H. Liu, R.C. Beardsley, An unstructured grid, finite-volume, three-dimensional, primitive equations ocean model: application to coastal ocean and estuaries, J. Atmos. Ocean. Technol. 20 (1) (2003) 159–186.
[29] L.C. Van Rijn, Principles of Sediment Transport in Rivers, Estuaries and Coastal Seas, 1006, Aqua publications Amsterdam, 1993.
[30] A. Iyer, S. Couch, G. Harrison, A. Wallace, Variability and phasing of tidal current energy around the United Kingdom, Renew. Energy 51 (2013) 343–357.
[31] A.J. Grass, Structural features of turbulent flow over smooth and rough boundaries, J. Fluid Mech. 50 (02) (1971) 233–255.
[32] L.O. Amoudry, P.S. Bell, P.D. Thorne, A.J. Souza, Toward representing wave-induced sediment suspension over sand ripples in rans models, J. Geophys. Res.: Oceans 118 (5) (2013) 2378–2392.
[33] G.R. Lesser, J.v. Roelvink, J. Van Kester, G. Stelling, Development and validation of a three-dimensional morphological model, Coast. Eng. 51 (8–9) (2004) 883–915.
[34] L.O. Amoudry, A.J. Souza, Impact of sediment-induced stratification and turbulence closures on sediment transport and morphological modelling, Cont. Shelf Res. 31 (9) (2011) 912–928.